

A Crossed Molecular Beams and Ab Initio Study on the Formation of C_6H_3 Radicals. An Interface between Resonantly Stabilized and Aromatic Radicals

R. I. Kaiser,* M. Goswami, P. Maksyutenko, F. Zhang, and Y. S. Kim

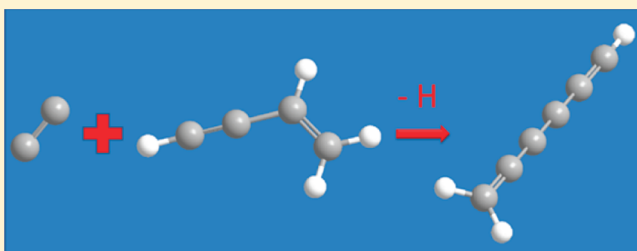
Department of Chemistry, University of Hawaii at Manoa, Honolulu, Hawaii 96822, United States

Alexander Landera and Alexander M. Mebel*

Department of Chemistry and Biochemistry, Florida International University, Miami, Florida 33199, United States

S Supporting Information

ABSTRACT: The crossed molecular beams reaction of dicarbon molecules, $C_2(X^1\Sigma_g^+ / a^3\Pi_u)$ with vinylacetylene was studied under single collision conditions at a collision energy of 31.0 kJ mol^{-1} and combined with electronic structure calculations on the singlet and triplet C_6H_4 potential energy surfaces. The investigations indicate that both reactions on the triplet and singlet surfaces are dictated by a barrierless addition of the dicarbon unit to the vinylacetylene molecule and hence indirect scattering dynamics via long-lived C_6H_4 complexes. On the singlet surface, ethynylbutatriene and vinylodiacetylene were found to decompose via atomic hydrogen loss involving loose exit transition states to form exclusively the resonantly stabilized 1-hexene-3,4-diynyl-2 radical (C_6H_3 ; $H_2CCCCCCH$; C_{2v}). On the triplet surface, ethynylbutatriene emitted a hydrogen atom through a tight exit transition state located about 20 kJ mol^{-1} above the separated stabilized 1-hexene-3,4-diynyl-2 radical plus atomic hydrogen product; to a minor amount ($<5\%$) theory predicts that the aromatic 1,2,3-tridehydrobenzene molecule is formed. Compared to previous crossed beams and theoretical investigations on the formation of aromatic C_6H_x ($x = 6, 5, 4$) molecules benzene, phenyl, and *o*-benzynes, the decreasing energy difference from benzene via phenyl and *o*-benzynes between the aromatic and acyclic reaction products, i.e., 253, 218, and 58 kJ mol^{-1} , is narrowed down to only $\sim 7 \text{ kJ mol}^{-1}$ for the C_6H_3 system (aromatic 1,2,3-tridehydrobenzene versus the resonantly stabilized free radical 1-hexene-3,4-diynyl-2). Therefore, the C_6H_3 system can be seen as a “transition” stage among the C_6H_x ($x = 6-1$) systems, in which the energy gap between the aromatic isomer ($x = 6, 5, 4$) is reduced compared to the acyclic isomer as the carbon-to-hydrogen ratio increases and the acyclic isomer becomes more stable ($x = 1, 2$).



1. INTRODUCTION

Resonantly stabilized free radicals (RSFRs) such as the propargyl radical (C_3H_3 ; H_2CCCH ; C_{2v})¹⁻⁵ and its higher homologous members 1-butene-3-yl-2 (C_4H_3 ; $H_2CCCCCH$; C_s),⁶ 2,4-pentadiynyl-1 (C_5H_3 ; $H_2CCCCCH$; C_{2v}),⁷⁻¹⁰ and the 1-hexene-3,4-diynyl-2 radical (C_6H_3 ; $H_2CCCCCCH$; C_{2v})¹¹ together with its methyl (CH_3), ethynyl (CCH), and vinyl (C_2H_3) substituted counterparts are considered important intermediates in the formation of polycyclic aromatic hydrocarbons (PAHs) and ultimately soot particles in combustion systems. In resonantly stabilized free radicals, the unpaired electron is delocalized over the carbon skeleton thus giving RSFRs their inherent thermodynamic stability. Together with monocyclic aromatic molecules such as benzene (C_6H_6),^{3,12,13} the phenyl radical (C_6H_5),¹⁴ and *o*-benzynes (*o*- C_6H_4),^{14,15} RSFRs can reach high concentrations in combustion flames. In these aromatic systems, the aromatic isomers are significantly more stable than the corresponding nonaromatic structures by 253, 218, and 58 kJ mol^{-1} for the C_6H_6 ,

C_6H_5 , and C_6H_4 potential energy surfaces (PESs), respectively, i.e., a decreasing energy gap between the aromatic and acyclic structures as the carbon-to-hydrogen ratio rises. On the other hand, recent crossed molecular beams and electronic structure calculations from our groups suggested that for the hydrogen deficient carbon clusters C_6H and C_6H_2 , the linear isomers 1,3,5-hexatriynyl-1 ($HCCCCC$)¹⁶ and triacetylene ($HCCCCCCH$)^{17,18} are energetically favored by 20 and 148 kJ mol^{-1} compared to their aromatic counterparts. Considering the difference in thermodynamical stability between the aromatic and nonaromatic, hydrogen rich ($x = 6, 5, 4$) and hydrogen depleted C_6H_x species ($x = 1, 2$), this makes the C_6H_3 system an interesting “transition” radical, in which the enhanced stability of the aromatic isomers (hydrogen rich) might switch to an energetically preferred

Received: June 20, 2011

Revised: July 26, 2011

Published: August 08, 2011

nonaromatic but resonantly stabilized free radical (hydrogen poor).

Previous experimental investigations of the C_6H_3 potential energy surface under single collision conditions focused solely on the reactions of singlet tricarbon molecules with methylacetylene (CH_3CCH) and allene (H_2CCCH_2), in which the C_{2v} symmetric 1-hexene-3,4-diynyl-2 radical (C_6H_3 ; $H_2CCCCCCH$) was formed as a consequence of a single collision event.¹⁹ In these previous studies, supporting electronic structure calculations did not consider any aromatic C_6H_3 isomers. Having demonstrated recently that the reactions of ethynyl (CCH) and singlet/triplet dicarbon (C_2) with 1,3-butadiene (C_4H_2) lead to the formation of—besides the acyclic isomers—benzene²⁰ and the phenyl radical²¹ and that the reaction of ethynyl (CCH) with vinylacetylene (C_4H_4) forms the aromatic *o*-benzynes¹⁵ molecule under collisionless conditions, it is logical to propose that bimolecular gas phase reactions of singlet and triplet dicarbon with vinylacetylene (C_4H_4) access various triplet and singlet C_6H_4 intermediates, which may decompose to aromatic (AR) and/or resonantly stabilized free radicals (RSFRs) of the molecular formula C_6H_3 . Therefore, we conducted the crossed molecular beam experiments of singlet and triplet dicarbon with vinylacetylene and combined the experimental results with electronic structure calculations on the singlet and triplet C_6H_4 potential energy surfaces to elucidate if ARs and/or RSFRs are the principal reaction products of these elementary reactions. We further discuss the role of the C_6H_3 system as the crucial link between energetically favored aromatic and resonantly stabilized radicals for hydrogen rich and poor C_6H_x molecules, respectively.

2. EXPERIMENTAL AND DATA PROCESSING

The experiments were carried out under single collision conditions utilizing a crossed molecular beams machine with in situ characterization of the dicarbon beam via laser induced fluorescence (LIF). Briefly, a pulsed dicarbon beam was generated in the primary source by laser ablation of graphite at 266 nm by focusing about 5 mJ per pulse on the rotating carbon rod. The ablated species were seeded in neat helium carrier gas (Gaspro, 99.9999%, 3040 Torr, Table 1) released by a Proch–Trickl pulsed valve operated at pulse widths of 80 μ s and -400 V. After the beam passed a skimmer, a four-slot chopper wheel mounted after the ablation zone selected a part of the seeded dicarbon beam, which then crossed a pulsed vinylacetylene beam (C_4H_4 , 99.5% purity) at seeding fractions of 5% in argon. Vinylacetylene itself was synthesized in our laboratory according to an adapted literature procedure.²²

As demonstrated earlier, at all velocities, the ablation beams contain dicarbon in its $X^1\Sigma_g^+$ electronic ground state as well as in its first electronically excited $a^3\Pi_u$ state.²³ Higher electronic excitations relax to one of the above-mentioned states during the ~ 30 μ s travel to the interaction region due to their short radiative lifetimes.²⁴ We characterized rovibrational energy distribution within both states employing laser induced fluorescence (LIF). Our in situ LIF detection setup has been described recently.²⁵ The singlet state was probed via Mulliken excitation ($D^1\Sigma_u^+ - X^1\Sigma_g^+$, ~ 231 nm) of (0,0) and (1,1) vibrational bands. Triplet states were monitored via Swan excitation ($d^3\Pi_g - a^3\Pi_u$, ~ 515 nm) of (0,0) and (1,1) vibrational bands. Swan transitions were excited by the fundamental pulsed 45 μ J output of a Lambda Physik Scanmate dye laser. Five microjoules of 231 nm radiation

Table 1. Peak Velocities (v_p), Speed Ratios (S), and the Center-of-Mass Angle (Θ_{CM}) along with the Nominal Collision Energy (E_c) of the Vinylacetylene with the Dicarbon Beam

	v_p (ms ⁻¹)	S	E_c (kJ mol ⁻¹)	Θ_{CM}
C_4H_4/Ar	642 ± 20	26.0 ± 1.0		
$C_2(a^3\Pi_u/X^1\Sigma_g^+)/He$	1834 ± 15	4.8 ± 0.2	31.0 ± 0.7	37.2 ± 0.7

for Mulliken band excitation has been produced in a Scanmate second harmonics generator fed by the output of the dye laser. The dye laser itself was pumped by the third harmonic of an integrated Nd:YAG laser operating at 10 Hz with an output power of 50 mJ per pulse. The fluorescence was detected by a Hamamatsu R955 photomultiplier tube (PMT) filtered by an Andover band-pass filter with 10 nm bandwidth centered at 560 and 230 nm for (1,0) or (2,1) Swan and (0,0) or (1,1) Mulliken fluorescence detection correspondingly. The signal was amplified by a built-in amplifier of the Hamamatsu C7247 PMT socket assembly and filtered by a high pass filter prior to feeding into a digital oscilloscope interfaced to a computer for data collecting and processing. The LIF spectra were then analyzed utilizing Diatomic spectral simulation program by Tan.²⁶ We adopted spectroscopic constants for the Swan band from Bernath^{27,28} and Schmidt and Bacskay²⁴ and from Sorkhabi et al.²⁹ for the Mulliken band.

Note that although the primary beam contains carbon atoms and tricarbon molecules as well, these species do not interfere with the ion counts of the dicarbon–vinylacetylene system at mass-to-charge ratios (m/z) of 75 ($C_6H_3^+$) and 74 ($C_6H_2^+$). Previous test experiments showed that tricarbon reacts with vinylacetylene only at collision energies larger than about 75–90 kJ mol⁻¹. Reactive scattering signal from the reaction of atomic carbon with vinylacetylene does not interfere either; only ion counts at m/z values of 63 ($C_5H_3^+$) and lower have been recorded in a previous study of this reaction.¹⁰

The reactively scattered species were monitored using a triply differentially pumped quadrupole mass spectrometric detector (QMS) in the time-of-flight (TOF) mode after electron-impact ionization of the neutral molecules at 80 eV electron energy. This detector can be rotated within the plane defined by the primary and the secondary reactant beams to allow recording angular resolved TOF spectra. By taking and integrating the TOF spectra, we obtain the laboratory angular distribution (LAB), which portrays the integrated signal intensity of an ion of distinct m/z versus the laboratory angle. To extract information on the chemical dynamics, the laboratory data (TOF and LAB distributions) were transformed into the CM frame and fit using a forward-convolution routine.^{30,31} This procedure initially assumes an angular distribution $T(\theta)$ and a translational energy distribution $P(E_T)$ in the CM reference frame (CM). TOF spectra and the laboratory angular distribution were then calculated from these $T(\theta)$ and $P(E_T)$ taking into account the beam spreads and the apparatus functions. Best fits of the TOF and laboratory angular distributions were achieved by refining the $T(\theta)$ parameters and the points of the $P(E_T)$.

3. THEORY

Geometric structures of local minima and transition states on the singlet and triplet C_6H_4 potential energy surfaces (PESs) pertinent to the reactions of dicarbon C_2 in its ground $^1\Sigma_g^+$ and excited $^3\Pi_u$ electronic states with vinylacetylene, as well as of the reactants and possible products, were optimized at the hybrid

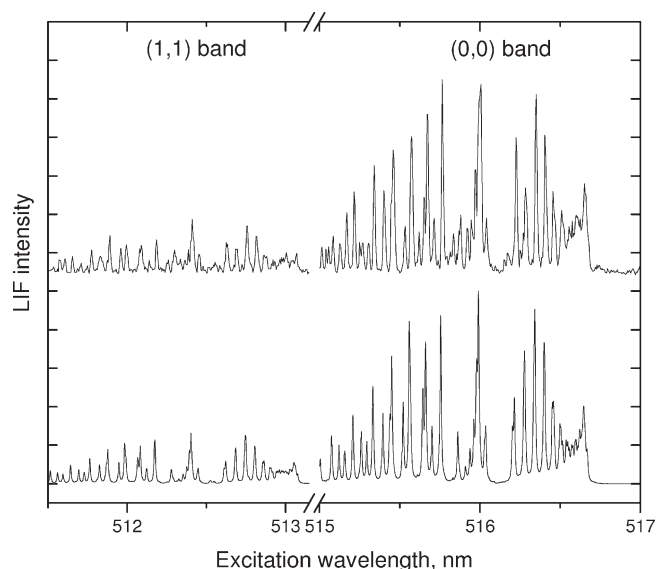


Figure 1. LIF excitation spectrum of the Swan band ($d^3\Pi_g - a^3\Pi_u$) in triplet dicarbon. Both the experimental spectrum (upper curve) and best-fit simulation (lower curve) are shown in the figure.

density functional B3LYP level with the 6-311G** basis set.^{32,33} Vibrational frequencies were calculated using the same B3LYP/6-311G** method and were utilized in computations of zero-point vibrational energy (ZPE) corrections and in statistical calculations of rate constants and product branching ratios. Relative energies of various species were refined employing the coupled cluster CCSD(T) method^{34–37} with extrapolation to the complete basis set (CBS) limit from total energy calculations with Dunning's correlation-consistent cc-pVDZ, cc-pVTZ, and cc-pVQZ basis sets,¹³ using the following formula, $E_{\text{tot}}(x) = E_{\text{tot}}(\infty) + Be^{-Cx}$, where x is the cardinal number of the basis set (2, 3, and 4) and $E_{\text{tot}}(\infty)$ is the CCSD(T)/CBS total energy.¹⁴ ZPEs obtained by B3LYP calculations were also included, and thus the overall level of theory used in this work is described as CCSD(T)/CBS//B3LYP/6-311G** + ZPE(B3LYP/6-311G**). All quantum chemical calculations were performed utilizing the GAUSSIAN 98³⁸ and MOLPRO³⁹ program packages. Optimized Cartesian coordinates of all structures involved in the reaction of dicarbon with vinylacetylene are collected in Table S1 of the Supporting Information along with rotational constants, vibrational frequencies, ZPE corrections, and CCSD(T) total energies. The results of the ab initio calculations, such as relative energies and molecular parameters, were utilized in RRKM and microcanonical variational transition state (VTST, for H elimination channels occurring without an exit barrier) calculations of energy-dependent rate constants, which in turn were used to compute product branching ratios at different collision energies.⁴⁰ Supporting Information shows minimal potential energy reaction profiles for barrierless H elimination reactions utilized in VTST calculations (S2) and also includes computed rate constants for unimolecular reaction steps and product branching ratios (Table S3, Supporting Information).

4. RESULTS

Excitation LIF spectra in Mulliken ($D^1\Sigma_u^+ - X^1\Sigma_g^+$) and Swan ($d^3\Pi_g - a^3\Pi_u$) bands (Figures 1 and 2) allow us to probe rovibrational state populations in singlet and triplet ablated

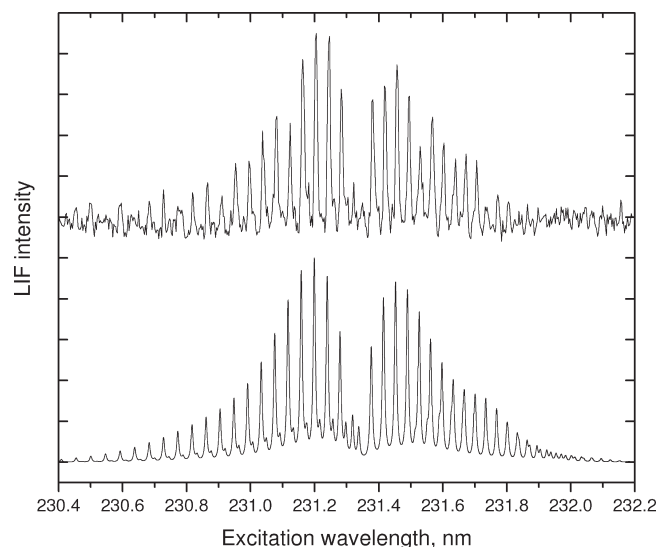


Figure 2. LIF excitation spectrum of Mulliken band ($D^1\Sigma_u^+ - X^1\Sigma_g^+$) in singlet dicarbon. Both the experimental spectrum (upper curve) and the best-fit simulation (lower curve) are shown in the figure.

Table 2. Vibrational and Rotational Energy Distribution in the Two Lowest Electronic States of Dicarbon

electronic state	$\nu = 0$	$\nu = 1$
$a^3\Pi_u$	(68 ± 10)% total:	(32 ± 8)% total:
	50 K, (45 ± 5)%	50 K, (20 ± 4)%
	300 K, (23 ± 5)%	300 K, (12 ± 4)%
$X^1\Sigma_g^+$	(83 ± 10)% total:	(17 ± 4)% total:
	200 K, (44 ± 5)%	200 K, (6 ± 2)%
	1000 K, (39 ± 5)%	1000 K, (11 ± 2)%

dicarbon cooled in helium supersonic expansion. The (0,0) and (1,1) vibrational bands are well separated energetically in the Swan system facilitating determination of relative $\nu = 0$ and $\nu = 1$ populations in the $a^3\Pi_u$ state. We did not observe the evidence of $\nu = 2$ being populated in either $a^3\Pi_u$ or $X^1\Sigma_g^+$ states. Table 2 summarizes relative vibrational populations within each state and rotational temperatures within each vibrational state inferred from comparison with best-fit spectral simulation. Similar to what have been reported earlier for our dicarbon ablation source,²⁵ rovibrational state distribution is nonequilibrium demanding two rotational temperatures in each vibrational state for an acceptable fit.

In the crossed beams experiments, we monitored reactive scattering signal at mass-to-charge ratios of $m/z = 75$ ($C_6H_3^+$), 74 ($C_6H_2^+$), and 73 (C_6H^+). After scaling, the TOF spectra of all three mass-to-charge ratios were superimposable suggesting that the molecular hydrogen elimination channel is closed and that signal at $m/z = 74$ and 73 originated from a dissociative ionization of the C_6H_3 parent radical in the ionizer of the detector by the 80 eV electrons (Figure 3). Therefore, the only reactive channel from dicarbon reactions observed in the present mass range is the formation of a molecule of the molecular formula C_6H_3 plus a hydrogen atom. The corresponding LAB angular distribution recorded at the most intense product ion of $m/z = 75$ is plotted in Figure 4. This distribution is spread over about 45° in the scattering plane defined by both the dicarbon

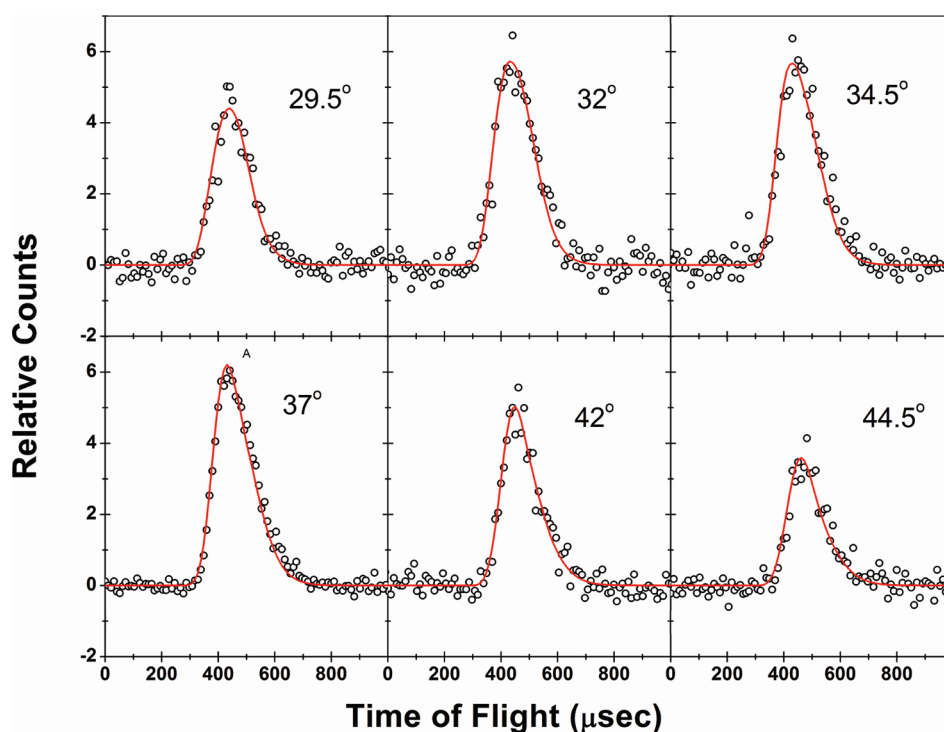


Figure 3. Selected time-of-flight spectra collected at $m/z = 75$ ($C_6H_3^+$) for the reaction of $C_2(X^1\Sigma_g^+/a^3\Pi_u)$ with vinylacetylene (C_4H_4) at various laboratory angles. Open circles represent the experimental data and the solid red lines indicate the fit.

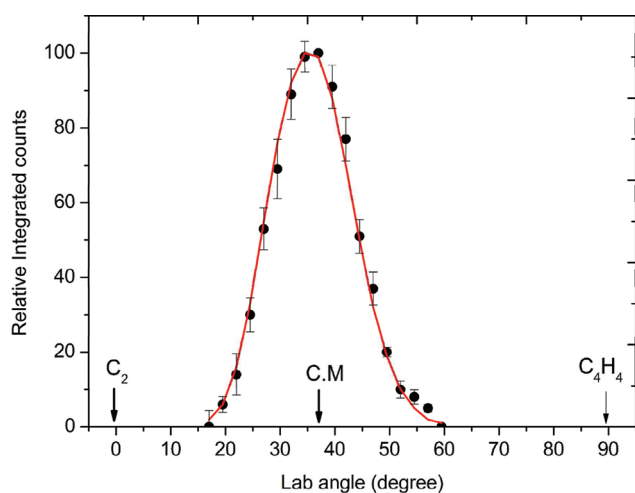


Figure 4. Laboratory angular distribution of the heavy reaction product for the reaction of $C_2(X^1\Sigma_g^+/a^3\Pi_u)$ with vinylacetylene (C_4H_4), monitored at $m/z = 75$ ($C_6H_3^+$). The solid circles represent the experimental data with the 1σ error bars. The center of mass (CM) angle is shown at 37.2° . The solid red line indicates the fits obtained from the best fit center of mass functions.

and vinylacetylene molecular beams. Also, the LAB distribution is almost symmetric with respect to the corresponding center-of-mass angle of $37.2 \pm 0.7^\circ$ and peaks close to the CM angle (Figure 4). This finding suggests that the reaction most likely involves a long-lived C_6H_4 reaction intermediate.

Having analyzed the laboratory data, we are turning our attention to the center-of-mass angular ($T(\theta)$) and translational energy distributions ($P(E_T)$) (Figures 5 and 6). Most importantly,

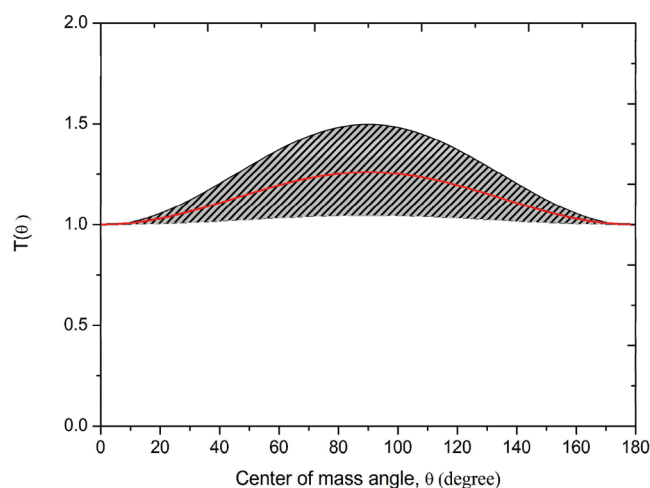


Figure 5. Center of mass angular distribution for the reaction of $C_2(X^1\Sigma_g^+/a^3\Pi_u)$ with vinylacetylene (C_4H_4) to form the C_6H_3 radical plus atomic hydrogen at collision energy of 31.0 kJ mol^{-1} . The hatched area represents the acceptable lower limit and the upper limit of the fit. The solid red line indicates the best fit.

the laboratory data could be fit with a single channel in point form of the mass combination 75 amu (C_6H_3) and 1 amu (H). The center-of-mass angular distribution (Figure 5) is essentially a forward–backward symmetric with respect to 90° . Best fit simulations yielded a distribution peaking at 90° ; however within the error limits, weakly polarized and essential flat distributions can fit the data as well. The intensity over the complete angular range indicates that the dicarbon–vinylacetylene system involves indirect scattering dynamics via the formation of bound C_6H_4

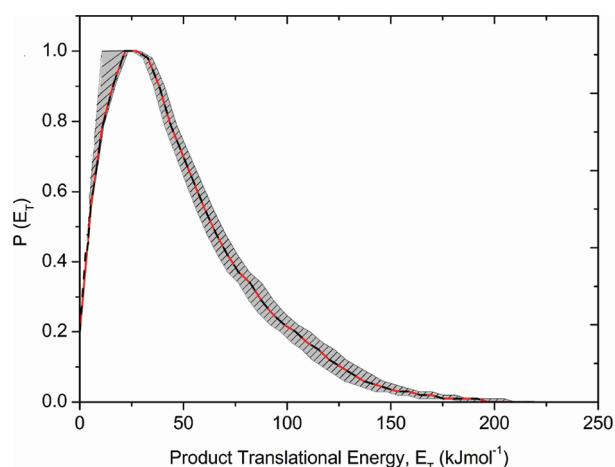


Figure 6. Translational energy distribution for the reaction of C_2 ($X^1\Sigma_g^+/a^3\Pi_u$) with vinylacetylene (C_4H_4) to form the C_6H_3 radical plus atomic hydrogen at collision energies of 32 kJ mol^{-1} . The hatched area represents the acceptable lower limit and the upper limit of the fit. The solid red line indicates the best fit functions.

reaction intermediate(s).⁴¹ Also, the inherent forward–backward symmetry of the $T(\theta)$ s suggests that the lifetime of the intermediate(s) is longer than its (their) rotational period or that the intermediate is symmetric.⁴¹ In the latter case, a rotational axis would interconvert both hydrogen atoms; this leads to an emission of atomic hydrogen with equal probability into θ° and $\pi-\theta^\circ$ and results in a forward–backward symmetric CM angular distribution. Further, the rather mild polarization is the effect of the poor coupling between the initial and final orbital angular momentum due to the light mass of the departing hydrogen atom.⁴¹ Angular momentum conservation suggests that most of the total, initial angular momentum channels into the rotational excitation of the polyatomic C_6H_3 product.

The center-of-mass translational energy distribution (Figure 6) provides further information to unravel the underlying chemical dynamics of the dicarbon–vinylacetylene reaction. First, the best fit $P(E_T)$ shows a small plateau-like structure from 10 to 27 kJ mol^{-1} . A comparison of related reactions of singlet and triplet dicarbon with acetylene⁴² and ethylene⁴³ suggests the presence of at least two exit channels (one from the singlet and triplet surface each) and that at least one channel involves a rather tight exit barrier. If the reaction only takes place on the singlet surface alone, a simple bond rupture process results in a peaking of the $P(E_T)$ close to zero translational energy; this has been clearly not observed. However, the involvement of the triplet surface is expected to result in a tight exit transition state with a repulsive bond rupture and hence off-zero peaking of the $P(E_T)$. The broad plateau, on the other hand, suggests a superposition of two exit channels, a loose and a tight exit transition state as observed in the related dicarbon–acetylene and dicarbon–ethylene systems. Our fits indicate that the tails of the $P(E_T)$ can be extended or shortened by up to 20 kJ mol^{-1} without significantly changing the results of the fit. Since the maximum translational energy presents the sum of the collision energy and the exoergicity of the reaction, the magnitude of E_{max} can be used to extract the reaction exoergicity. Here, we determine that the formation of C_6H_3 and the hydrogen atom is exoergic by $169 \pm 25 \text{ kJ mol}^{-1}$. As demonstrated by our LIF studies, the dicarbon reactants are in the singlet and also in the first excited triplet state. Here, the

enthalpy of formation of $C_2(a^3\Pi_w, \nu = 0)$ is higher by 7.3 kJ mol^{-1} compared to $C_2(X^1\Sigma_g^+, \nu = 0)$. Therefore, on the triplet surface, the reaction is exoergic by $176 \pm 25 \text{ kJ mol}^{-1}$. Note that there is a possible role of rovibrational excitation of the dicarbon reactant that has not been accounted for so far. For instance, the first vibrational level of dicarbon in both electronic states has an energy content of about $19\text{--}22 \text{ kJ mol}^{-1}$. On the basis of the LIF studies, one quanta of vibrational energy can be stored as vibrational energy content of dicarbon; this likely alters the value of the reaction energy and increases the uncertainty. This shifts the reaction energies to lower values than mentioned above to 149 ± 27 and $156 \pm 27 \text{ kJ mol}^{-1}$ for the singlet and triplet surfaces, respectively, if the vibrational energy is released as translational energy. Finally, from the center-of-mass translational energy distribution, we can also compute the fraction of the energy on average channeling into the translational modes of the products, to be about $35 \pm 5\%$. This order of magnitude indicates indirect scattering dynamics.⁴¹

5. DISCUSSION

Having established that a species of the molecular formula C_6H_3 plus atomic hydrogen is formed and that the molecular hydrogen channel yielding C_6H_2 isomer(s) is closed, we are attempting now to unravel the nature of the isomer(s) formed. For this, we are comparing the experimentally determined reaction energies of $169 \pm 25 \text{ kJ mol}^{-1}$ (singlet surface) and $176 \pm 25 \text{ kJ mol}^{-1}$ (triplet surface) with the theoretically predicted ones (Figure 7). On both the singlet and triplet surfaces, the computations predict the formation of four possible isomers: the aromatic 1,2,3-tridehydrobenzene, 1,2,4-tridehydrobenzene, and 1,3,5-tridehydrobenzene listed with decreasing order of thermodynamical stability as well as the resonantly stabilized free radical 1-hexene-3,4-diynyl-2. Note that the 1,2,3-tridehydrobenzene is close in energy to the 1-hexene-3,4-diynyl-2 radical isomer and only favored by $6\text{--}7 \text{ kJ mol}^{-1}$. The experimentally determined reaction energy of $169 \pm 25 \text{ kJ mol}^{-1}$ lies very close to the predicted energies of the 1-hexene-3,4-diynyl-2 radical and of the 1,2,3-tridehydrobenzene as well as 1,2,4-tridehydrobenzene; the situation is identical for the triplet surface. Since these aromatic and resonantly stabilized C_6H_3 radicals are too close in energy, which is well within our experimental error limits, we have to concede that our experiments alone cannot determine which isomer(s) is (are) formed under single collision conditions. Therefore, we inspect the underlying potential energy surfaces for guidance (Figure 7) and compare the predicted mechanism(s) with our experimental data.

On the singlet surface, the reaction proceeds indirectly via complex formation without entrance barrier. Similar to the reactions of dicarbon with acetylene and ethylene studied earlier in our group,^{42,43} dicarbon can add to the acetylenic and/or vinyl moieties of the vinylacetylene molecule yielding collision complexes **si1** (addition to CCH) and/or **si2** and **si3** (addition to C_2H_3) to either two or to the terminal carbon atom, respectively. Note that **si2** can ring open to **si3**. Theory predicts that these initial collision complexes are connected to seven singlet reaction intermediates: two acyclic closed shell molecules ethynylbutatriene (**si4**) and vinylodiacetylene (**si5**), *o*-, *m*-, and *p*-benzynes (**si6–8**), and two nonaromatic cyclic structures **si9** and **si10**. Intermediate **si2** most likely isomerizes to **si3**, which in turn undergoes ring closure to **si10**; **si1** can isomerize predominantly to **si9**. Considering the barrier to isomerization of **si10** to **si4** and **si7**, we can predict that **si4** is formed preferentially; **si9** can only

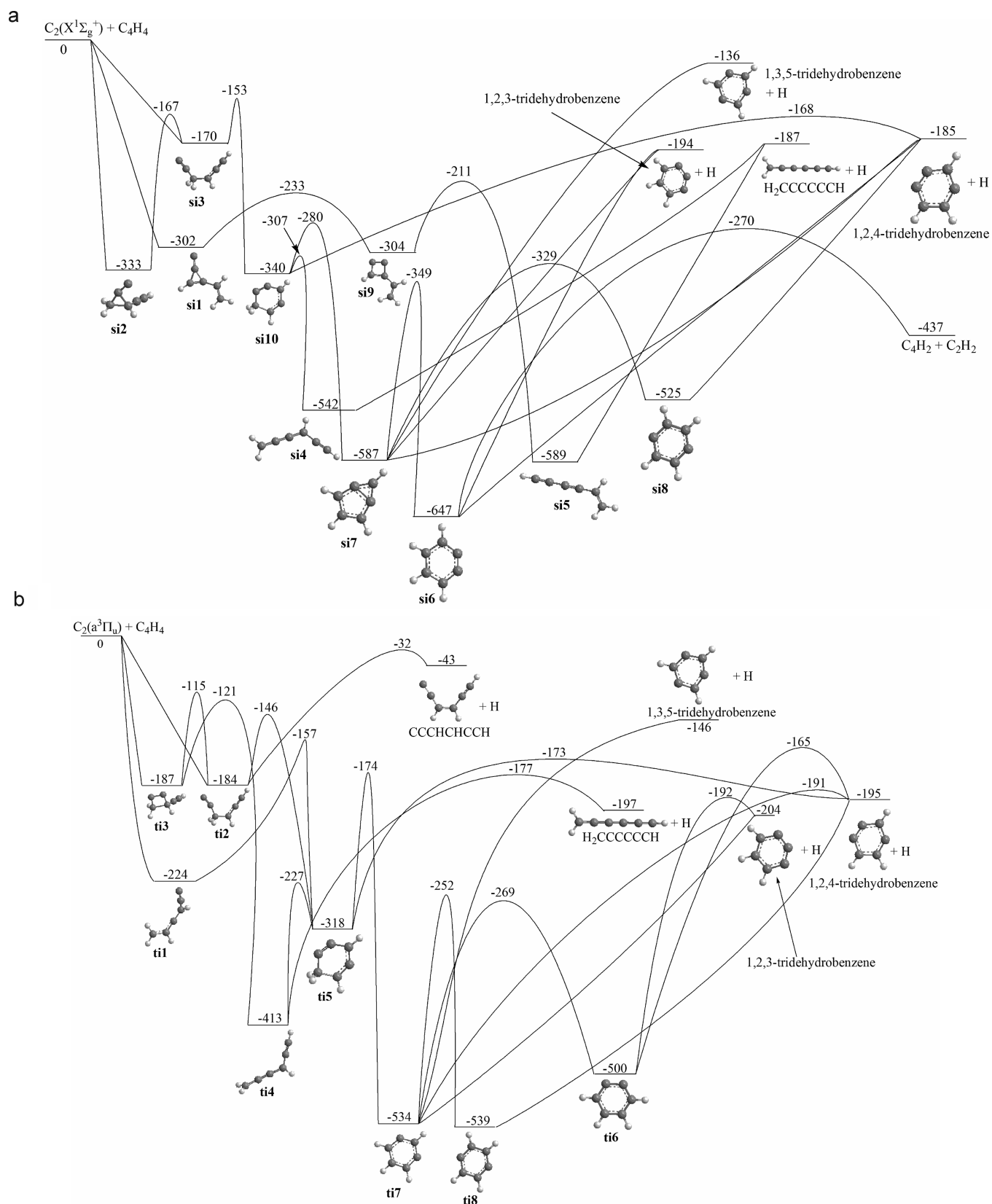


Figure 7. (a) Potential energy diagram of the $C_2(X^1\Sigma_g^+) + C_4H_4$ reaction calculated at the CCSD(T)/CBS//B3LYP/6-311G** level of theory. (b) Potential energy diagram of the $C_2(a^3\Pi_u) + C_4H_4$ reaction calculated at the CCSD(T)/CBS//B3LYP/6-311G** level of theory. All relative energies are given in kJ mol^{-1} .

ring open to **si5**. Therefore, it is likely that all initial collision complexes **si1**–**si3** formed via addition of the dicarbon molecule

to the π -system lead eventually to two acyclic isomers: **si4** and **si5**. Both intermediates can undergo atomic hydrogen emission

to form the resonantly stabilized 1-hexene-3,4-diynyl-2 radical without exit barrier through loose transition states. These considerations are fully supported by our RRKM calculations. These predict that on the singlet surface, the 1-hexene-3,4-diynyl-2 radical is formed almost exclusively among the C_6H_3 products and the results are nearly independent of the collision energy. Although the tridehydrobenzenes are close in energy to the RSFR, they cannot be accessed due to the significantly enhanced barrier involved in the isomerization of, for instance, **si10** to **si4** compared to **si7** (*m*-benzyne). In addition, if **si7** is formed, it prefers to isomerize to *o*-benzyne **si6**, and the most favorable decomposition channel of the latter is C_4H_2 (diacetylene) + C_2H_2 (acetylene) rather than 1,2,3-tridehydrobenzene plus atomic hydrogen. On the basis of RRKM calculations, diacetylene plus acetylene contribute up to 9% to the total product yield.

On the triplet surface, the situation is more complex. Triplet dicarbon can add in analogy to the reactions of triplet dicarbon with acetylene and ethylene either to the acetylenic moiety forming **ti1** or to one or both carbon atoms of the vinyl group yielding triplet intermediates **ti2** and **ti3**, respectively, with a facile isomerization of **ti2** to **ti3**. These three collision complexes can isomerize yielding eventually five reaction intermediates: triplet ethynylbutatriene (**ti4**), the nonaromatic, cyclic intermediate **ti5**, and three triplet benzyne (ortho, meta, and para, **ti6–8**). Considering the isomerization barriers of the initial collision complexes, we may suggest that **ti1** ring-closures preferentially to **ti5**, which then ring opens to the acyclic intermediate **ti4**. Similarly, **ti2** isomerizes favorably to **ti5**, which then ring opens to **ti4**. Hence we can predict that **ti5** presents the central reaction intermediate which rearranges to the acyclic triplet structure **ti4**. The latter can eject a hydrogen atom involving a tight exit transition state located 20 kJ mol^{-1} above the separated atomic hydrogen plus 1-hexene-3,4-diynyl-2 radical products. However, compared to the singlet surface, two alternative isomerization pathways from **ti5** might involve transition states which are located 53 and 54 kJ mol^{-1} higher in energy compared to the one leading to **ti4**. These two competing pathways are expected to be less favorable due to the higher isomerization barrier, but one of them might lead to triplet *m*-benzyne, which can successively isomerize to *o*- and *p*-benzyne. Alternatively, **ti5** can eject a hydrogen atom through a tight transition state forming 1,2,4-tridehydrobenzene; 1,2,3- and 1,3,5-tridehydrobenzene can also be accessed via decomposition of the corresponding benzyne intermediates. Similar to the singlet surface, we conducted RRKM calculations. The results are in line with our discussion showing that the 1-hexene-3,4-diynyl-2 radical presents the dominant product (>95%), but minor contributions of the 1,2,4-tridehydrobenzene molecule are predicted (~4% at low collision energies but less than 1% at the collision energy of our experiment).

Can these predicted mechanisms account for the experimental findings? First of all, the computations predict only the emission of atomic hydrogen, but not of molecular hydrogen. This agrees nicely with our experimental findings. Second, the shape of the center-of-mass translational energy distributions suggested the involvement of two reaction channels involving loose and tight exit transition states. The calculations indicate that the barrierless decomposition of **si4** and **si5** can present a mechanism involving no exit barrier and hence a loose exit transition state on the singlet surface. On the triplet surface, the predicted decomposition of **ti4** via a tight exit transition state located 20 kJ mol^{-1} above the separated products can be

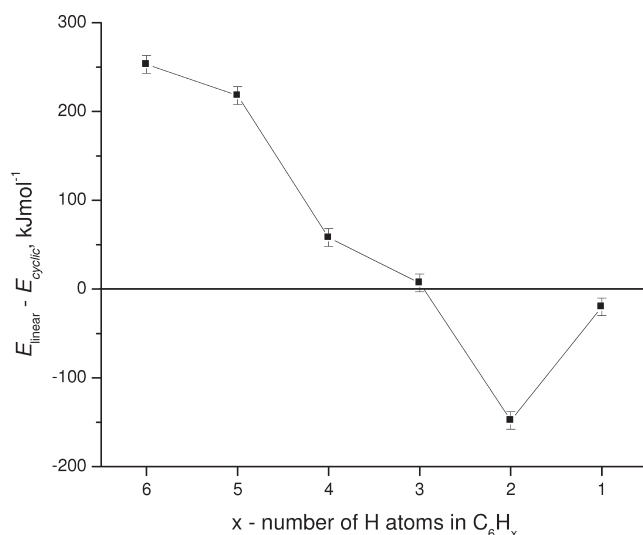


Figure 8. Energy differences between the aromatic isomer and their acyclic structures for the C_6H_x ($x = 6-1$) systems. The energy gap decreases as the carbon-to-hydrogen ratio increases and stabilizes the non-aromatic isomer for $x = 2$ and 1 compared to the aromatic structure for $x = 3-6$. The expected accuracy for the energy differences is within 10 kJ mol^{-1} .

identified as the second reaction channel involving a tight exit transition state. Third, these hydrogen emissions dominate the indirect, complex forming reaction dynamics involving at least three steps.

6. SUMMARY

We studied the crossed molecular beams reaction of dicarbon molecules, $C_2(X^1\Sigma_g^+/a^3\Pi_u)$ with vinylacetylene under single collision conditions at a collision energy of 31.0 kJ mol^{-1} and combined the experimental data with novel electronic structure calculations on the singlet and triplet C_6H_4 potential energy surfaces (PESs). The investigations suggest that both reactions on the triplet and singlet surfaces are dictated by a barrierless addition of the dicarbon unit to the vinylacetylene molecule and hence indirect scattering dynamics via long-lived C_6H_4 complexes. On the singlet surface, ethynylbutatriene and vinyl diacetylene were found to decompose via atomic hydrogen loss involving loose exit transition states to form exclusively the resonantly stabilized 1-hexene-3,4-diynyl-2 radical (C_6H_3 , $H_2CCCCCCH$, C_{2v}). On the triplet surface, ethynylbutatriene emitted a hydrogen atom through a tight exit transition state located about 20 kJ mol^{-1} above the separated stabilized 1-hexene-3,4-diynyl-2 radical plus atomic hydrogen product; to a minor amount (<5%) theory predicts that the aromatic 1,2,3-tridehydrobenzene molecule is formed. Compared to previous crossed beams and theoretical investigations of the formation of aromatic C_6H_x ($x = 6, 5, 4$) products benzene, phenyl, and *o*-benzyne, the decreasing energy difference from benzene via phenyl and *o*-benzyne between the aromatic and acyclic reaction product, i.e., 253, 218, and 58 kJ mol^{-1} , is further narrowed to only $\sim 7 \text{ kJ mol}^{-1}$ for the C_6H_3 system (aromatic 1,2,3-tridehydrobenzene versus the resonantly stabilized free radical 1-hexene-3,4-diynyl-2) (Figure 8). Therefore, the C_6H_3 isomers represent the “transition” system among the C_6H_x ($x = 6-1$) systems, in which the energy gap between the aromatic isomer ($x = 6, 5, 4$) is reduced compared to the acyclic isomer as the carbon-to-hydrogen ratio increases. Note that considering the significant internal energy

(rotation and vibration) of the 1-hexene-3,4-diynyl-2 radical (C_6H_3 , $H_2CCCCCCH$, C_{2v}) product of about 150 kJ mol^{-1} on average, it is interesting to see if this primary product can isomerize to the 1,2,4-tridehydrobenzene molecule. This isomerization requires a three-step pathway with the highest barrier ranging at about 256 kJ mol^{-1} above the 1-hexene-3,4-diynyl-2 radical.⁴³ Therefore, only for those 1-hexene-3,4-diynyl-2 radicals with a significant internal excitation, the 1,2,4-tridehydrobenzene molecule might be accessible.

■ ASSOCIATED CONTENT

S Supporting Information. Total molecular energies at the CCSD(T) level extrapolated to the complete basis set (CBS) limit, zero-point energy corrections (ZPE), rotational constants, molecular geometries, and vibrational frequencies of all stationary points (Table S1), potential energy curves along the minimal energy paths for barrierless hydrogen elimination channels (S2), and unimolecular rate constants for various reaction steps on the singlet and triplet surfaces calculated using RRKM theory or VTST at various collision energies and product branching ratios under single-collision conditions (Table S3). This material is available free of charge via the Internet at <http://pubs.acs.org>.

■ ACKNOWLEDGMENT

This work was supported by the US Department of Energy, Basic Energy Sciences (DE-FG02-03ER15411 to the University of Hawaii) and DE-FG02-04ER15570 to Florida International University).

■ REFERENCES

- (1) Kaiser, R. I.; Lee, Y. T.; Suits, A. G. *J. Chem. Phys.* **1996**, *105*, 8705–8720.
- (2) Miller, J. A.; Klippenstein, S. J.; Georgievskii, Y.; Harding, L. B.; Allen, W. D.; Simmonett, A. C. *J. Phys. Chem. A* **2010**, *114*, 4881–4890.
- (3) Pope, C. J.; Miller, J. A. *Proc. Combust. Inst.* **2000**, *28*, 1519–1527.
- (4) Miller, J. A.; Klippenstein, S. J. *J. Phys. Chem. A* **2003**, *107*, 7783–7799.
- (5) Scherer, S.; Just, T.; Frank, P. *Proc. Combust. Inst.* **2000**, *28*, 1511–1518.
- (6) Kaiser, R. I. *Abstracts of Papers*, 224th ACS National Meeting, Boston, MA, United States, August 18–22, 2002; American Chemical Society: Washington, DC, 2002; PHYS-071.
- (7) Guo, Y.; Gu, X.; Balucani, N.; Kaiser, R. I. *J. Phys. Chem. A* **2006**, *110*, 6245–6249.
- (8) Guo, Y.; Gu, X.; Zhang, F.; Mebel, A. M.; Kaiser, R. I. *J. Phys. Chem. A* **2006**, *110*, 10699–10707.
- (9) Hansen, N.; Klippenstein, S. J.; Miller, J. A.; Wang, J.; Cool, T. A.; Law, M. E.; Westmoreland, P. R.; Kasper, T.; Kohse-Hoeinghaus, K. *J. Phys. Chem. A* **2006**, *110*, 4376–4388.
- (10) Parker Dorian, S. N.; Zhang, F.; Kim, Y. S.; Kaiser Ralf, I.; Mebel Alexander, M. *J. Phys. Chem. A* **2011**, *115*, 593–601.
- (11) Guo, Y.; Gu, X.; Zhang, F.; Mebel, A. M.; Kaiser, R. I. *Phys. Chem. Chem. Phys.* **2007**, *9*, 1972–1979.
- (12) Westmoreland, P. R.; Dean, A. M.; Howard, J. B.; Longwell, J. P. *J. Phys. Chem.* **1989**, *93*, 8171–8180.
- (13) Kern, R. D.; Wu, C. H.; Yong, J. N.; Pamidimukkala, K. M.; Singh, H. J. *Energy Fuels* **1988**, *2*, 454–457.
- (14) Li, Y.; Zhang, L.; Tian, Z.; Yuan, T.; Zhang, K.; Yang, B.; Qi, F. *Proc. Combust. Inst.* **2009**, *32*, 1293–1300.

- (15) Zhang, F.; Parker, D.; Kim, Y. S.; Kaiser, R. I.; Mebel, A. M. *Astrophys. J.* **2011**, *728*, 141/141–141/110.
- (16) Zhang, F.; Kim, S.; Kaiser, R. I.; Mebel, A. M. *J. Phys. Chem. A* **2009**, *113*, 1210–1217.
- (17) Gu, X.; Kim, Y. S.; Kaiser, R. I.; Mebel, A. M.; Liang, M. C.; Yung, Y. L. *Proc. Natl. Acad. Sci. U.S.A.* **2009**, *106*, 16078–16083.
- (18) Sun, B. J.; Huang, C. H.; Tsai, M. F.; Sun, H. L.; Gao, L. G.; Wang, Y. S.; Yeh, Y. Y.; Shih, Y. H.; Sia, Z. F.; Chen, P. H.; et al. *J. Chem. Phys.* **2009**, *131*, 104305.
- (19) Guo, Y.; Gu, X.; Zhang, F.; Mebel, A. M.; Kaiser, R. I. *Phys. Chem. Chem. Phys.* **2007**, *9*, 1972–1979.
- (20) Jones, B. M.; Zhang, F.; Kaiser, R. I.; Jamal, A.; Mebel, A. M.; Cordiner, M. A.; Charnley, S. B. *Proc. Natl. Acad. Sci. U.S.A.* **2011**, *108*, 452–457.
- (21) Zhang, F.; Jones, B.; Maksyutenko, P.; Kaiser, R. I.; Chin, C.; Kislov, V. V.; Mebel, A. M. *J. Am. Chem. Soc.* **2010**, *132*, 2672–2683.
- (22) Kim, Y. S.; Kaiser, R. I. *Astrophys. J., Suppl. Ser.* **2009**, *181*, 543–547.
- (23) Kaiser, R. I.; Le, T. N.; Nguyen, T. L.; Mebel, A. M.; Balucani, N.; Lee, Y. T.; Stahl, F.; Schleyer, P. v. R.; Schaefer, H. F., III *Faraday Discuss.* **2001**, *119*, 51–66.
- (24) Schmidt, T. W.; Bacskay, G. B. *J. Chem. Phys.* **2008**, *127*, 234310.
- (25) Kaiser, R. I.; Paksyutenko, P.; Ennis, C.; Zhang, F.; Gu, X.; Krishtal, S.; Mebel, A. M.; Kostko, O.; M., A. *Faraday Discuss.* **2010**, *147*, 429–478.
- (26) Tan, X. *Diatom, 1.4.1.1*; CyberWit: Santa Clara, CA, 2004.
- (27) Prasad, C. V. V.; Bernath, P. F. *Astrophys. J.* **1994**, *426*, 812–821.
- (28) Tanabashi, A.; Hirao, T.; Amano, T.; Bernath, P. F. *Astrophys. J., Suppl. Ser.* **2007**, *169*, 472–484.
- (29) Sorkhabi, O.; Xu, D. D.; Blunt, V. M.; Lin, H.; Roosevelt, P.; Wrobel, J. D.; Jackson, W. M. *J. Mol. Spectrosc.* **1998**, *188*, 200–208.
- (30) Vernon, M. *Ph.D. Thesis*, University of California, Berkeley, 1981.
- (31) Weiss, M. S. *Ph.D. Thesis*, University Of California, Berkeley, 1986.
- (32) Becke, A. D. *J. Chem. Phys.* **1993**, *98*, 5648–5652.
- (33) Lee, C.; Yang, W.; Parr, R. G. *Phys. Rev. B: Condens. Matter Mater. Phys.* **1988**, *37*, 785–789.
- (34) Purvis, G. D., III; Bartlett, R. J. *J. Chem. Phys.* **1982**, *76*, 1910–1918.
- (35) Scuseria, G. E.; Janssen, C. L.; Schaefer, H. F., III *J. Chem. Phys.* **1988**, *89*, 7382–7387.
- (36) Scuseria, G. E.; Schaefer, H. F., III *J. Chem. Phys.* **1989**, *90*, 3700–3703.
- (37) Pople, J. A.; Head-Gordon, M.; Raghavachari, K. *J. Chem. Phys.* **1987**, *87*, 5968–5975.
- (38) Frisch, M. J.; Trucks, G. W.; Schlegel, H. B.; Scuseria, G. E.; Robb, M. A.; Cheeseman, J. R.; Zakrzewski, V. G.; Montgomery, J. A.; Stratmann, R. E.; Burant, J. C.; Dapprich, S. et al. *Gaussian 98, revision A.11*; Gaussian, Inc.: Pittsburgh, PA, 1998.
- (39) *MOLPRO, version 2002.1*, a package of ab initio programs; Werner, H.-J.; Knowles, P. J.; Amos, R. D.; Bernhardsson, A.; Berning, A.; Celani, P.; Cooper, D. L.; Deegan, M. J. O.; Dobbyn, A. J.; Eckert, F.; Hampel, C.; Hetzer, G.; Knowles, P. J.; Korona, T.; Lindh, R.; Lloyd, A. W. et al. See <http://www.molpro.net>.
- (40) Kislov, V. V.; Nguyen, T. L.; Mebel, A. M.; Lin, S. H.; Smith, S. C. *J. Chem. Phys.* **2004**, *120*, 7008–7017.
- (41) Levine, R. D. *Molecular Reaction Dynamics*; Cambridge University Press, Cambridge, U.K., 2005.
- (42) Kaiser, R. I.; Balucani, N.; Charkin, D. O.; Mebel, A. M. *Chem. Phys. Lett.* **2003**, *382*, 112–119.
- (43) Mebel, A. M.; Kisiov, V. V.; Kaiser, R. I. *J. Chem. Phys.* **2006**, *125*, 133113.